Internal Radionuclide Radiation Dosimetry: A Review of Basic Concepts and Recent Developments*

Pat B. Zanzonico

Nuclear Medicine Service, Memorial Sloan-Kettering Cancer Center, New York, New York

Internal dosimetry deals with the determination of the amount and the spatial and temporal distribution of radiation energy deposited in tissue by radionuclides within the body. Nuclear medicine has been largely a diagnostic specialty, and model-derived average organ dose estimates for risk assessment, the traditional application of the MIRD schema, have proven entirely adequate. However, to the extent that specific patients deviate kinetically and anatomically from the model used, such dose estimates will be inaccurate. With the increasing therapeutic application of internal radionuclides and the need for greater accuracy, radiation dosimetry in nuclear medicine is evolving from population- and organ-average to patient- and position-specific dose estimation. Beginning with the relevant quantities and units, this article reviews the historical methods and newly developed concepts and techniques to characterize radionuclide radiation doses. The latter include the 3 principal approaches to the calculation of macroscopic nonuniform dose distributions: dose point-kernel convolution, Monte Carlo simulation, and voxel S factors. Radiation dosimetry in "sensitive" populations, including pregnant women, nursing mothers, and children, also will be reviewed.

Key Words: dosimetry; MIRD; radionuclide therapy

J Nucl Med 2000; 41:297–308

Internal radionuclide radiation dosimetry deals with the determination of the amount and spatial and temporal distribution of radiation energy deposited in tissue by radionuclides within the body. Internal dosimetry has been applied to the determination of tissue doses and related quantities for occupational exposures in radiation protection, environmental exposures in radiation epidemiology, and diagnostic and therapeutic exposures in nuclear medicine. Historically, nuclear medicine has been largely a diagnostic specialty, and the associated risk–benefit analyses implicitly performed by the clinician have been straightforward. Relatively low administered activities yield important diagnostic information, the benefits of which far outweigh any potential risk associated with the attendant normal-tissue radiation doses. Such small risk-to-benefit ratios have been very forgiving of possible inaccuracies in dose estimates.

By incorporation of radionuclides in appropriately large amounts into target tissue–avid radiopharmaceuticals, a sufficiently high radiation dose may be delivered to produce a therapeutic response in tumor or other target tissue. With escalating administered activities and associated normal-tissue doses, serious radiation injury can ensue, however. It becomes imperative, then, that the magnitude of the target tissue and at-risk normal tissue radiation doses be established with reasonable accuracy and precision and used in conjunction with reliable dose–response relationships for target tissues and dose–toxicity relationships for normal tissues. With the ongoing development of new radiopharmaceuticals and the increasing therapeutic application of internal radionuclides (particularly in the form of radioimmunotherapy), radiation dosimetry in nuclear medicine continues to evolve from population- and organ-average to patient- and position-specific dose estimation (*1–3*). Patient-specific dosimetry refers to the estimation of radiation dose to tissues of a specific patient, based on his or her individual body habitus and measured radiopharmaceutical kinetics rather than on an average anthropomorphic model and hypothetic kinetics. In contrast to the average dose, position-specific dosimetry refers to radiation doses to specific points in a tumor or organ and thus reflects the spatial variation in dose within a target tissue. This article reviews the historical methods and newly developed concepts and techniques to characterize radionuclide radiation doses.

STOCHASM AND DETERMINISM

Dosimetric quantities may be characterized as stochastic or deterministic (i.e., nonstochastic). A quantity subject to statistical fluctuations because of the small number of energy deposition events contributing to the quantity or the small volume of the region for which the quantity is being determined is termed "stochastic." The mean, or expectation value, of a large number of determinations of a

Received Sep. 20, 1999; revision accepted Oct. 12, 1999.

For correspondence or reprints contact: Pat B. Zanzonico, PhD, Nuclear Medicine Service, Memorial Sloan-Kettering Cancer Center, 1275 York Ave., New York, NY 10021.

*NOTE: FOR CE CREDIT, YOU CAN ACCESS THIS ARTICLE ON THE SNM WEB SITE (http://www.snm.org) UNTIL AUGUST 2000.

stochastic quantity is termed "deterministic." Each stochastic quantity thus has a corresponding, generally more familiar, deterministic quantity.

The field of microdosimetry deals with the number, size, and spatial and temporal distributions of individual energy-deposition events, particularly in submicroscopic structures (*4–6*). Increasingly, radiation dosimetry in nuclear medicine deals with the nonuniformity of dose within organs, among cells, and even within cells. Even so, dose is still almost always expressed in terms of deterministic quantities, and such dosimetry should therefore not be referred to as microdosimetry. Terms such as "small-scale dosimetry" or "cell-level dosimetry" would be more appropriate. However, the nonuniformity of energy deposition associated with α-ray emitters (*7,8*) and with radioimmunotherapy (*9*) may warrant the rigorous application of microdosimetry (*10*).

RADIATION QUANTITIES AND UNITS

Definitions of various quantities used to specify radiation dose and of selected related quantities are presented here. A compilation of System Internationale (SI) and conventional quantities and their symbols, units, and conversion factors are presented elsewhere (*6,11*).

Administered Activity

Administered activity is specified by the SI unit becquerel, equaling 1 disintegration/s (dps) or some multiple thereof. The conventional unit of activity, the Curie, corresponds to 3×10^{10} dps. Note that 37 MBq equals 1 mCi and 37 kBq equals 1 μCi. It is important to distinguish the radiation dose from the administered activity, with the former quantity taking into account the radionuclide and its physical characteristics, tissue mass, and the radiopharmaceutical and its kinetics as well as the administered activity.

Absorbed Dose and Specific Energy

Perhaps the most widely used and biologically meaningful quantity for expressing radiation dose, the absorbed dose (D), is defined as:

$$D \equiv \frac{d\bar{E}}{dm}, \qquad \text{Eq. 1}$$

where $d\bar{E}$ = the mean energy imparted by ionizing radiation to matter and dm = the mass of matter to which the energy is imparted.

The absorbed dose, defined for all ionizing radiations in any stopping medium, is the deterministic correlate of the stochastic quantity, specific energy (z_1):

$$z_1 \equiv \frac{\epsilon_1}{m}, \qquad \text{Eq. 2}$$

where ϵ_1 = the energy imparted to matter by a single energy-deposition event and m = the mass of the matter.

The unit of absorbed dose and specific energy is the same: the SI unit is the gray (1 Gy = 1 J/kg), and the conventional unit is the rad (1 rad = 100 erg/g); 1 Gy equals 100 rad, and 1 rad equals 1 cGy (or 10 mGy) (*11*).

Linear Energy Transfer and Lineal Energy

The quality and the quantity of radiation are important determinants of the frequency or severity of radiogenic biologic effects. The quality of a radiation is related to the characteristics of the microscopic spatial distribution of energy-deposition events. Sparsely ionizing radiations, such as x- and γ-rays and intermediate- to high-energy electrons and β-rays, are characterized as low-quality radiations. Densely ionizing radiations, such as low-energy electrons (e.g., Auger electrons), protons, neutrons, and α-rays, are typically characterized as high-quality radiations. For the same absorbed dose, the frequency or severity of biologic effects is generally less for sparsely ionizing than for densely ionizing radiations.

The quality of radiation is characterized by the linear energy transfer (L or LET):

$$L \equiv \frac{dE}{dl}, \qquad \text{Eq. 3}$$

where dE = the energy lost by a charged particle (or the secondary charged particle produced by the primary radiation) in traversing a distance in matter and dl = the distance traversed in matter.

LET is the deterministic correlate of the stochastic quantity, lineal energy (y):

$$y \equiv \frac{\epsilon_1}{\bar{l}}, \qquad \text{Eq. 4}$$

where ϵ_1 = the energy imparted to matter by a single energy-deposition event and $\bar{l}$ = the mean chord length of the volume of matter.

The unit of linear energy transfer and lineal energy is the same: the SI unit is the J/m and the conventional unit is the keV/μm; 1 J/m equals 6.25×10^9 keV/μm, and 1 keV/μm equals 1.60×10^{-10} J/m (*11*).

Relative Biologic Effectiveness

The influence of LET on the frequency or severity of biologic effects is quantified by the relative biologic effectiveness (RBE):

$$RBE(A) \equiv \frac{D_{reference}}{D_A}, \qquad \text{Eq. 5}$$

where $D_{reference}$ = the absorbed dose of reference radiation (typically a widely available, sparsely ionizing radiation, such as cobalt-60 γ-rays) required to produce a specific, quantitatively expressed biologic effect and D_A = the absorbed dose of radiation A required to produce the same frequency or severity of the same specific biologic effect, with all pertinent parameters maintained as nearly identical as possible. The RBE is a ratio of absorbed doses and thus is a dimensionless quantity.

Radiation Weighting Factor and Equivalent Dose

A simplified version of the RBE, the radiation weighting factor (w_R), was devised for purposes of radiation protection (Table 1). The so-called equivalent dose (H_T) in tissue or organ T is related to the radiation weighting factors (w_R) and the mean absorbed doses ($D_{T,R}$) to tissue or organ T from radiations (R):

$$H_T \equiv \sum_R w_R D_{T,R} . \qquad \text{Eq. 6}$$

The w_R and H_T are similar, respectively, to the older quantities of quality factor (Q) and dose equivalent (H). The key difference is that the former are related to the mean dose to a tissue or organ, whereas the latter are related to the dose at a point and thus are often less useful.

Tissue Weighting Factor and Effective Dose

The effective dose (E) is intended to provide a single-value estimate of the overall stochastic risk (i.e., the total risk of cancer and genetic defects) of a given irradiation, whether received by the whole body, part of the body, or 1 or more individual organs:

$$E \equiv \sum_T w_T H_T \qquad \text{Eq. 7}$$

$$= \sum_T \sum_R w_T w_R D_{T,R} , \qquad \text{Eq. 8}$$

where w_T = the weighting factor for tissue or organ T, a dimensionless quantity representing the fraction contributed by tissue or organ T to the total stochastic risk (i.e., the combined total risks of cancer or of severe hereditary defects for all subsequent generations) as the result of a uniform, total-body irradiation (Table 2). The effective dose is similar in concept to the effective dose equivalent (H_E) introduced previously by the International Commission on Radiation Units and Measurements (*12*) and the National Council on Radiation Protection (*13*) and representing a single-value estimate of the net harm from any low-dose (e.g., diagnostic nuclear medicine) exposure. However, the dose equivalent is based on the absorbed dose at a point in tissue weighted by the LET-dependent distribution of quality factors at that point. The equivalent dose, in contrast, is based on the average absorbed doses in the tissue or organ weighted by the radiation weighting factor for the radiation actually impinging on that tissue or organ. The effective dose and the effective dose equivalent do not apply to, and should not be used for, high-dose (e.g., therapeutic nuclear medicine) exposures (*14*).

The unit of equivalent dose and effective dose is the same: the SI unit is the sievert and the conventional unit is the rem; 1 Sv equals 100 rem, and 1 rem equals 1 cSv (or 10 mSv) (*13*). w_R and w_T are dimensionless quantities (Tables 1 and 2) (*15,16*).

TABLE 1
w_R for Calculation of H_T to Tissue or Organ

Type and energy range	w_R
X and γ-rays, electrons, positrons, and muons*	1
Neutrons, energy	
<10 keV	5
10–100 keV	10
>100 keV–2 MeV	20
>2–20 MeV	10
>20 MeV	5
Protons† other than recoil protons and energy > 2 MeV	2‡
α particles, fission fragments, nonrelativistic heavy nuclei	20

*Excluding Auger electrons emitted from nuclei bound to DNA, because averaging dose in this case is unrealistic. Techniques of microdosimetry are more appropriate in this case.

†In circumstances in which human body is irradiated directly by >100-MeV protons, RBE is likely to be similar to that of low–linear energy transfer radiation, and, therefore, w_R of approximately unity would be appropriate for that case.

‡w_R value for high-energy protons recommended here is lower than that recommended by International Commission on Radiological Protection (1991).

All values relate to radiation incident on body or, for internal sources, emitted from source. Adapted with permission of (*16*).

THE TRADITIONAL MIRD SCHEMA

The methodology now widely used used for internal dose calculations in medicine, including age- and sex-specific reference data for human anatomy and body composition, was developed by the MIRD committee of the Society of Nuclear Medicine and is generally referred to as the MIRD schema or MIRD formalism (*2,17–19*). The International Commission on Radiological Protection (ICRP) has developed a similar methodology and similar reference data (*20*).

The MIRD schema, including notation, terminology, mathematic methodology, and reference data, has been disseminated in the form of the collected MIRD pamphlets and associated publications (*2,17–19*). With the publication of work by Christy and Eckerman (*21*), age- and sex-specific body habiti other than the original 70-kg adult anthropomorphic model (known as "Standard Man") (*22*) now are incorporated into the MIRD schema. In addition, several computerized versions of the MIRD schema have been developed, including MIRDOSE (*23*), DOSCAL (which incorporates mean tumor doses) (*24*), and MABDOS (with curve fitting and modeling features) (*25–27*).

In its traditional application to diagnostic radiopharmaceuticals, the MIRD schema implicitly assumes that activity and cumulated activity are uniformly distributed within organ size source regions and that radiation energy is uniformly deposited within organ size target regions. Moreover, dosimetry for diagnostic radiopharmaceuticals is generally based on (a) average time–activity data in animal models or in small cohorts of human subjects and (b) age- and sex-specific "average" models of human anatomy. The traditional MIRD schema does not incorporate tumors as either source or target regions.

TABLE 2
w_T for Tissue or Organ for Calculation of Effective Dose

w_T	Tissue or organ
0.01	Bone surface, skin
0.05	Bladder, breast, liver, esophagus, thyroid, remainder*
0.12	Bone marrow, colon, lung, stomach
0.20	Gonads

*For purposes of calculation, remainder is composed of the following additional tissues and organs: adrenals, brain, small intestine, large intestine, kidney, muscle, pancreas, spleen, thymus, and uterus. List includes organs that are likely to be selectively irradiated. Some organs in list are known to be susceptible to cancer induction. If other tissues and organs subsequently become identified as having significant risk of induced cancer, they will then be included either with a specific w_T or in this additional list constituting remainder. Remainder may also include other tissues or organs selectively irradiated. In those exceptional cases in which 1 remainder tissue or organ receives equivalent dose in excess of highest dose in any of the 12 organs for which weighting factor is specified, weighting factor of 0.025 should be applied to that tissue or organ and weighting factor of 0.025 to average dose in other remainder tissues or organs.

Values have been developed for reference population of equal numbers of both sexes and wide range of ages. In definition of effective dose, they apply to workers, to whole population, and to either sex. These w_T values are based on rounded values of organ's contribution to total detriment. Adapted with permission of (*16*).

BEYOND THE TRADITIONAL MIRD SCHEMA

The traditional MIRD schema has proven invaluable for dosimetric risk assessment in diagnostic nuclear medicine. However, to the extent that specific patients deviate kinetically and anatomically from the respective kinetic and anatomic averages, tissue dose estimates will be inaccurate. Robert Loevinger, an originator of the MIRD schema, has stated that, ". . .there is in principle no way of attaching a numerical uncertainty to the profound mismatch between the patient and the model (the totality of all assumptions that enter into the dose calculation). The extent to which the model represents in some meaningful way a patient, or a class of patients, is always open to question, and it is the responsibility of the clinician to make that judgment"(*19*). Because of the large risk–benefit ratios associated with diagnostic radiopharmaceuticals, any inaccuracies (perhaps up to 100% [2]) in tissue absorbed dose estimates for individual patients probably are unimportant. With therapeutic radiopharmaceuticals, however, the risk-benefit ratios are dramatically smaller, and the tolerances for inaccuracies in dose estimation are greatly reduced.

With the growth of radionuclide therapy, various techniques beyond the traditional MIRD schema have been developed to improve the accuracy of dose estimates, including techniques for patient- and position-specific radiation dosimetry. Any perception that such techniques somehow correct inherent limitations of the MIRD schema is mistaken, however. Indeed, a remarkable strength of the MIRD schema is its generality: by judicious selection of source and target regions, it can be used to calculate the dose to virtually any structure from virtually any activity distribution, from microscopic to macroscopic to whole organ and whole body. With the publication of MIRD *Cellular S Factors* (*28*), the MIRD schema has been extended to cellular and subcellular source and target regions, with the cell and the nucleus modeled as unit density concentric spheres of radius 3–10 and 1–8 μm, respectively. More recently, MIRD pamphlet no. 17, *The Dosimetry of Nonuniform Activity Distributions: Radionuclide S Values at the Voxel Level* (*29*) has extended the MIRD schema to arbitrary macroscopic activity distributions in 3 dimensions for calculation of the resulting macroscopic dose distribution. In this context, macroscopic refers to volume elements (or voxels) 3 mm or greater in dimension. In both publications, the distance-dependent photon and electron dose contributions are included and, in the case of β-rays, the actual energy spectra (versus simply the mean energy) are used.

Patient-Specific Dosimetry

Individual variations in radiopharmaceutical kinetics may result in substantial deviations from population-average dose estimates, so that they are not predictive of target tissue response or normal tissue toxicity in radionuclide therapy. This is illustrated by the various dosimetric approaches to radioiodine treatment of hyperthyroidism (*30*).

The clinical effectiveness of radioiodine treatment of hyperthyroidism is presumably related to the absorbed dose to thyroid follicular cells. Yet, the most common dose prescription algorithm, a fixed administered activity, entails administration of a specified activity (currently, approximately 370 MBq [10 mCi]) to all hyperthyroid patients. By ignoring those highly variable individual parameters (i.e., thyroid uptake, biologic half-life, and mass) that determine absorbed dose, it is unlikely that there will be a correlation between the administered activity and the absorbed dose (Fig. 1). Although up to 85% of patients will eventually be "cured" (i.e., made euthyroid or hypothyroid) by the administration of single doses of standard amounts of radioiodine (and presumably 100% of patients treated with repeated administrations) (*31*), such an arbitrary approach does not permit individually optimized therapy and would not identify patients such as "small-pool" patients for whom radioiodine therapy may be inappropriate or even hazardous.

Prescription of a specified activity concentration (typically 2000–3000 MBq/g [55–80 μCi/g]) in the thyroid incorporates 2 important dosimetric variables, thyroid uptake and mass, into calculation of the administered activity but implicitly assumes a constant thyroid half-life of radioiodine:

$$\text{administered activity} = \frac{\text{prescribed activity concentration} \times \text{gland mass (g)} \times 100}{\text{24-h \% uptake}}. \quad \text{Eq. 9}$$

A prescribed absorbed dose (Gy [rad]) is the dose

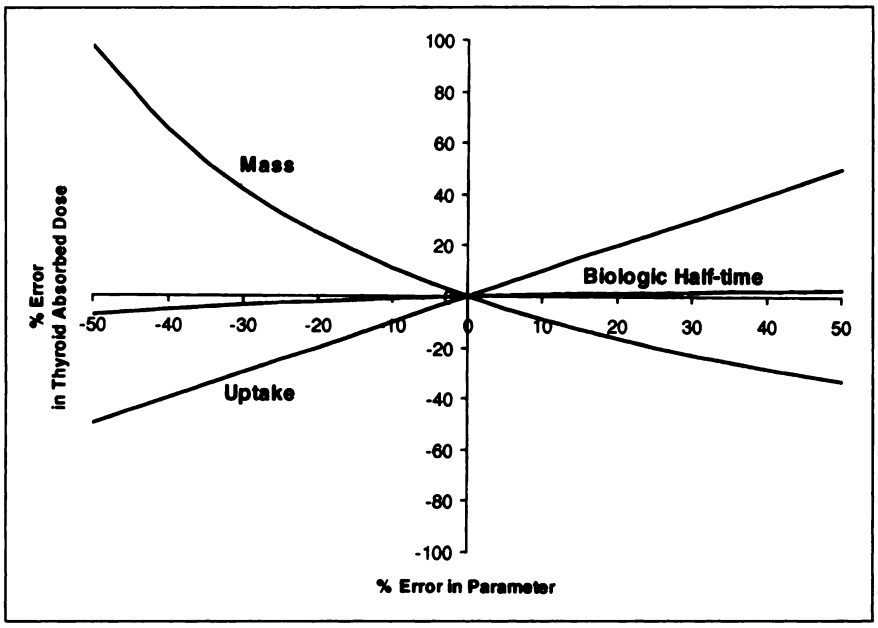

FIGURE 1. Relative error in calculated ^{131}I absorbed dose to thyroid as function of relative error in thyroid 24-h uptake, biologic half-life, and mass. Baseline parameters are 24-h uptake of 25%, biologic half-life of 90 d, and mass of 21 g. Note that, for errors in biologic half-life, relative error in thyroid absorbed dose becomes important only for very large negative errors. For example, if actual biologic half-life were only 5 d (typical of small pool patients), actual thyroid dose would be overestimated by ~60% if one assumes standard biologic half-life of 90 d.

prescription algorithm presently used least often, because it requires serial uptake measurements and is therefore time consuming. However, it is the most logical dosimetrically, incorporating all pertinent and practically evaluable parameters into the calculation of the administered activity:

administered activity (kBq) =

$$\frac{\text{prescribed absorbed dose (cGy)} \times \text{gland mass (g)} \times 6.67 \times 37}{(T_{1/2})_{eff}\,\text{(day)} \times \text{24-h \% uptake}}, \quad \text{Eq. 10}$$

where $(T_{1/2})_{eff}$ = the effective half-life of radioiodine in the thyroid, which in turn equals

$$\frac{(T_{1/2})_p \times (T_{1/2})_b}{(T_{1/2})_p + (T_{1/2})_b}, \quad \text{Eq. 11}$$

where $(T_{1/2})_b$ = the biologic (or radioactive decay-corrected) half-life of radioiodine in the thyroid, and $(T_{1/2})_p$ = the physical half-life of ^{131}I (8.04 d). Implicit in Equation 10 are the assumptions that the only significant absorbed dose to the thyroid is from self-irradiation, all nonpenetrating radiations (i.e., β-rays) emitted within the thyroid are completely absorbed locally, and the proportion of thyroid mass attributable to lymphocytes is negligible. The factor of 6.67 was derived by Marinelli et al. (*32–34*) (a) assuming the thyroid to have a mass of 25 g and to consist of 2 unit density tangent spheres, each of mass 12.5 g and radius (R) of 1.44 cm, yielding a mean geometric factor ($\bar{g}_{sphere}$) 3 π R of 12.3 cm; (b) assuming radioiodine in the thyroid follows a monoexponential time–activity function; (c) using a mean β-ray energy of 0.191 MeV and a specific γ-ray constant of 0.00223 R cm^2/mCi/h (in conventional units) for ^{131}I; and (d) incorporating the appropriate unit conversion factors. (The factor for converting μCi to kBq, 37, is presented explicitly to retain the familiar factor of 6.67 in the Marinelli formulation.) Because the ^{131}I γ-rays typically contribute <10% of the dose, deviations of thyroid masses from the assumed value of 25 g have only a minor effect on the thyroid dose calculated using Equation 9.

The following have been offered as general guidelines for single-dose radioiodine therapy of hyperthyroidism (*35,36*): for young patients and those with uncomplicated Graves' disease (i.e., small glands and mild to moderate hyperthyroidism), 7,000–8,000 rad; for patients with complicated Graves' disease (i.e., larger glands and more severe hyperthyroidism), 10,000–12,000 rad; and for patients with toxic nodular goiter, 15,000–25,000 rad. However, in contrast to typical hyperthyroid patients ($[T_{1/2}]_b$ = 20–25 d), 15% of hyperthyroid patients have a more rapid thyroidal turnover of radioiodine ($[T_{1/2}]_b$ = 5–10 d). This is thought to be the result of a small thyroidal iodine pool (small-pool syndrome). As a result, serum protein-bound radioiodine, the source of as much as 90% of the ^{131}I blood absorbed dose, is elevated (to as high as 2% of the administered activity per liter of serum), with a resulting increase in the blood absorbed dose. At the same time, the thyroid absorbed dose is reduced because radioiodine is more rapidly secreted from, and therefore has less time to irradiate, the thyroid. The relatively small thyroidal absorbed dose in small-pool patients is probably responsible for at least some failures of radioiodine treatment. Barandes et al. (*37*), for example, reported a series of 7 small-pool hyperthyroid patients in whom a standard 7000-cGy (7000-rad) thyroid absorbed dose would require the administration of 1040 MBq (28 mCi) ^{131}I (in contrast to only 120 MBq (3.2 mCi) typically required) and theoretically deliver a blood absorbed dose of 150 cGy (150 rad), a prohibitively high incidental dose for treatment of a benign disease.

A general patient-specific treatment-planning paradigm is as follows (*30,38–42*). A tracer (diagnostic) amount of the

therapeutic radiopharmaceutical is administered to the patient. Serial time–activity measurements are performed for blood, tumor, or other target tissue; critical normal organs; or the total body (*30,41,43,44*). These kinetic data are integrated to determine the corresponding cumulated activities (or residence times), and the absorbed doses per unit administered activity are calculated. The actual therapeutic administered activity is that projected to deliver maximum tolerated doses to 1 or more critical normal tissues or, less commonly, a minimum effective dose to tumor or other target tissue. For ^{131}I-iodide treatment of metastatic thyroid cancer, for example, the therapeutic administered activity is that calculated to deliver no more than 2 Gy (200 rad) to blood (as a surrogate for bone marrow) (*30,41,45,46*). In radioimmunotherapy of non-Hodgkin's B-cell lymphoma with ^{131}I-labeled anti-B1 (anti-CD20) monoclonal antibody, on the other hand, the therapeutic administered activity is that delivering a dose of 0.75 Gy (75 rad) to the total body (again as a surrogate for bone marrow) (*47–50*). For radiolabeled monoclonal antibody and other targeted therapies in which uptake is saturable or otherwise nonlinear, with varying "mole" amounts administered, mathematic (e.g., compartmental) modeling of the tracer kinetic data may be useful in determining the optimum amount (mole or mg) as well as activity of the therapeutic radiopharmaceutical (*51–57*). After the therapeutic administration, serial time–activity measurements and cumulated-activity and absorbed-dose calculations may be repeated and the projected and actual therapeutic absorbed doses compared.

Nonuniform Dose Distributions

Normal tissue toxicity and tumor therapeutic response may not correlate with average doses, even when based on individualized kinetics. Thus, in addition to patient-specific dosimetry, the issue of spatial nonuniformity of dose has become increasingly important at the macroscopic (*29,58–77*) and microscopic (*78–96*) levels.

Potential radiogenic damage to the hematopoietic bone marrow is the primary dose-limiting toxicity for systemic radionuclide therapy in general and radioimmunotherapy in particular (*45,97,98*). A variety of approaches have therefore been pursued in an effort to establish a predictive dose–response relationship for myelotoxicity in radioimmunotherapy (*97,99–101*). Although no such correlation has proven especially useful (*50,102–107*), absorbed dose yields a better correlation than administered activity. Moreover, marrow absorbed dose appears to be a marginally better predictor of myelotoxicity than whole-body absorbed dose. However, in an intermediate absorbed-dose range, myelotoxicity has been unpredictable. This may be a notable example of the inadequacy of the average dose as a quantitative descriptor of tissue irradiation and potential toxicity (Fig. 2).

Nonuniformity of dose in target tissues such as tumor likewise may make it difficult to reliably predict therapeutic response in radionuclide therapy. O'Donoghue (*108*) has modeled the impact of dose nonuniformity (*109*) on radiocurability of tumors. As shown in Figure 3, tumor response is poorer (i.e., tumor cell survival is greater) as dose nonuniformity increases. The dose–response curve is concave upward (Fig. 3D), indicating that the tumor-sparing effect of dose nonuniformity is greatest at higher doses. A substantial fraction of tumor cells will therefore receive sublethal doses, and the tumor may therefore not regress, even if the average tumor dose is sufficiently high to otherwise create an expectation of a significant therapeutic response. A clinically predictive average dose–response curve may be difficult or impossible to derive in the face of such nonuniformity.

There are at least 3 approaches to the calculation of macroscopic nonuniform dose distributions (*29*): dose point-kernel convolution, Monte Carlo simulation, and voxel S factors. The dose point-kernel is currently the most widely used of these approaches (*42,60–63,73,110*), primarily because of the demanding computational requirements of

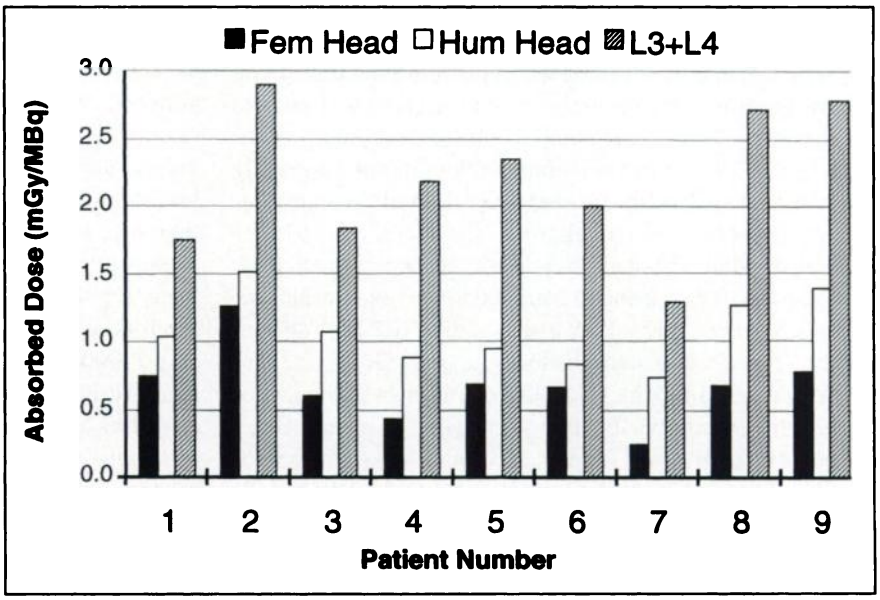

FIGURE 2. Nonuniformity of bone marrow absorbed dose. Absorbed dose per unit administered activity (mGy/MBq) to bone marrow in femoral heads (Fem Head), humeral heads (Hum Head), and lumbar vertebrae 3 and 4 (L3+L4) was evaluated in 9 patients with leukemia who received 300 MBq ^{131}I-labeled HuM195 anti-CD33 monoclonal antibody. Note 2- to 3-fold variation in estimated absorbed doses among 3 marrow sites. (Adapted with permission of (*131*).)

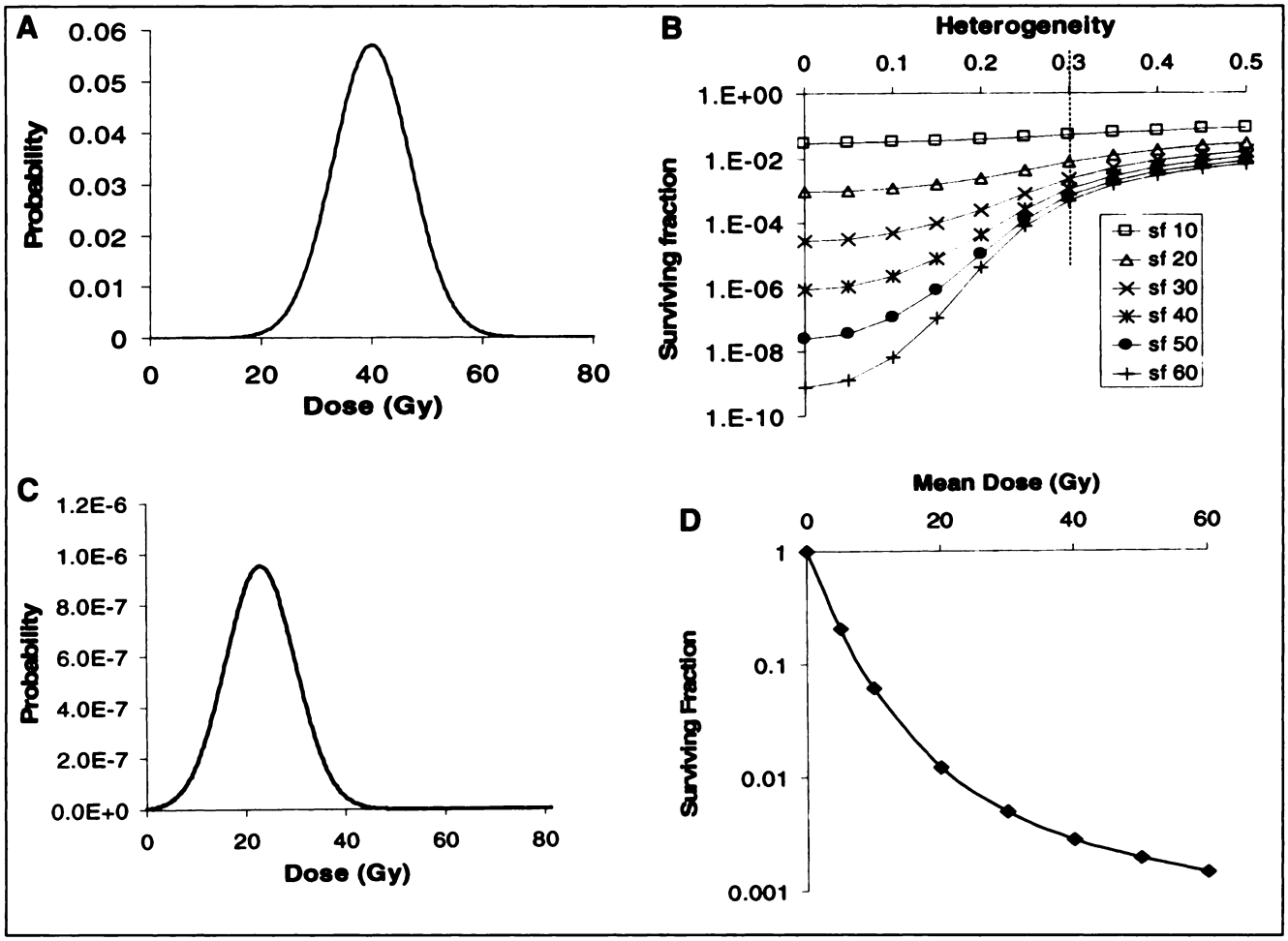

FIGURE 3. Effect of dose nonuniformity on tumor response (*108*). (A) Hypothetic nonuniform dose to tumor cell population represented by normal distribution (*109*) with average of 40 Gy, SD of 7 Gy, and fractional SD (FSD) of 7/40 Gy = 0.175. (B) Tumor cell survival probability for dose distribution in (A), assuming monoexponential tumor cell survival curve with mean lethal dose (D_0) of 2.85 Gy (i.e., α = 0.35/Gy). Overall tumor cell survival fraction is represented by area under curve. (C) Overall tumor cell survival fraction as function of dose nonuniformity expressed as FSD of average dose from 0 (i.e., uniform dose) to 0.5 and of average tumor dose from 10 Gy (highest curve) to 60 Gy (lowest curve). Tumor cell survival is greater as dose nonuniformity increases. (D) Dose–response for dose nonuniformity (i.e., FSD) of 0.35, corresponding to points intersecting dotted vertical line, is concave upward. (Adapted with permission of (*108*).)

Monte Carlo simulation and the limited availability of voxel S factors. (A dose point-kernel is the radial distance-dependent absorbed dose about an isotropic point source in an infinite homogeneous medium [typically a soft tissue–equivalent medium such as water].) With the wider availability of high-speed desktop computers and of compatible simulation codes, the use of Monte Carlo analysis may increase (*58,59,111*). Monte Carlo–based dosimetry can more accurately account for tissue variations in mass density and atomic number as well as edge effects, which may be important at the periphery of the body and at soft tissue–lung and –bone interfaces (*58*). For example, if the relevant microscopic distribution data were somehow available (e.g., by autoradiography of biopsy specimens), Monte Carlo analysis might be especially applicable to normal lung dosimetry in radioiodine treatment of metastatic thyroid cancer, particularly in dosimetrically problematic miliary disease. This method remains computationally time consuming, however (*58*). Tabulations of voxel S factors, conceptually equivalent to voxel source-kernels (the mean absorbed dose to a target voxel per radioactive decay in a source voxel, both of which are contained in an infinite homogeneous soft-tissue medium) (*76,77*), are becoming available (*29*). In contrast to techniques based on the dose point-kernel and Monte Carlo simulation, the voxel S factor method does not require specialized computer facilities and is relatively fast. Thus, it may emerge as the practical method of choice for calculation of macroscopic nonuniform dose distributions.

Once a dose distribution has been calculated, a corresponding dose–volume histogram can be derived. A dose–volume histogram is a graph of the fraction of the tumor or organ volume receiving a specified dose versus the dose (differential form) or the fraction of the tumor or organ volume receiving less than a specified dose versus the dose (integral or cumulative form) (Fig. 4). It therefore graphically presents

the minimum, mean, and maximum doses and the dispersion about the mean dose. The greater this dispersion, the more nonuniform is the dose distribution.

An important practical component of macroscopic nonuniform dosimetry is the ability to fuse, or register, tomographic images from multiple modalities (*67,112–115*). Dose distributions, calculated from 3-dimensional activity distributions measured by scintigraphic imaging (i.e., SPECT or PET), may be presented as isodose contours (Fig. 4) or color-coded images (Fig. 5). By image fusion, such isodose contours or color-coded images can be superimposed on or juxtaposed with the corresponding anatomy to allow correlation of doses with tumor and normal organs (as imaged by CT or MRI) (*29,60,76,114*).

"SENSITIVE" POPULATIONS

The administration of certain radioactive materials, even in diagnostic amounts, to certain sensitive populations, including pregnant females, nursing mothers, and children, remains a matter of concern in nuclear medicine.

Pregnant Females

By modification of the standard anthropomorphic adult phantom (*21,22*), increasingly accurate anatomic models of the fetus and pregnant female have been developed. These include models of the pregnant female at the beginning of pregnancy (representing the embryo as a small unit density sphere located at the uterus) (*116*) and at the end of the first and third trimesters (*117*). Radiopharmaceutical kinetic data in utero and, therefore, fetal dose estimates are quite limited, however. Published fetal absorbed-dose estimates are generally ≤0.1 cGy (0.1 rad)/37 mBq (1 mCi) administered to the mother (*116,118–122*).

A particularly worrisome issue is radioiodine administration to pregnant females (*123,124*). The fetal thyroid begins concentrating iodine at 12–15 wk of gestation. At 16–24 wk, ^{131}I-iodide delivers a very large absorbed dose of 1500–6000 cGy/37 MBq to the fetal thyroid and an absorbed dose of 3–5 cGy/37 MBq to the fetal total body, depending on maternal thyroid uptake (*124*). For a hyperthyroid therapy administration of 185 MBq (5 mCi), 7,500–30,000 cGy (rad) would therefore be delivered to the fetal thyroid and 15–25 rad to the fetal total body. Not surprisingly, with radiogenic destruction of the fetal thyroid and thyroid hormone deficiency in utero, fetal hypothyroidism and congenital cretinism have been shown to result after radio-

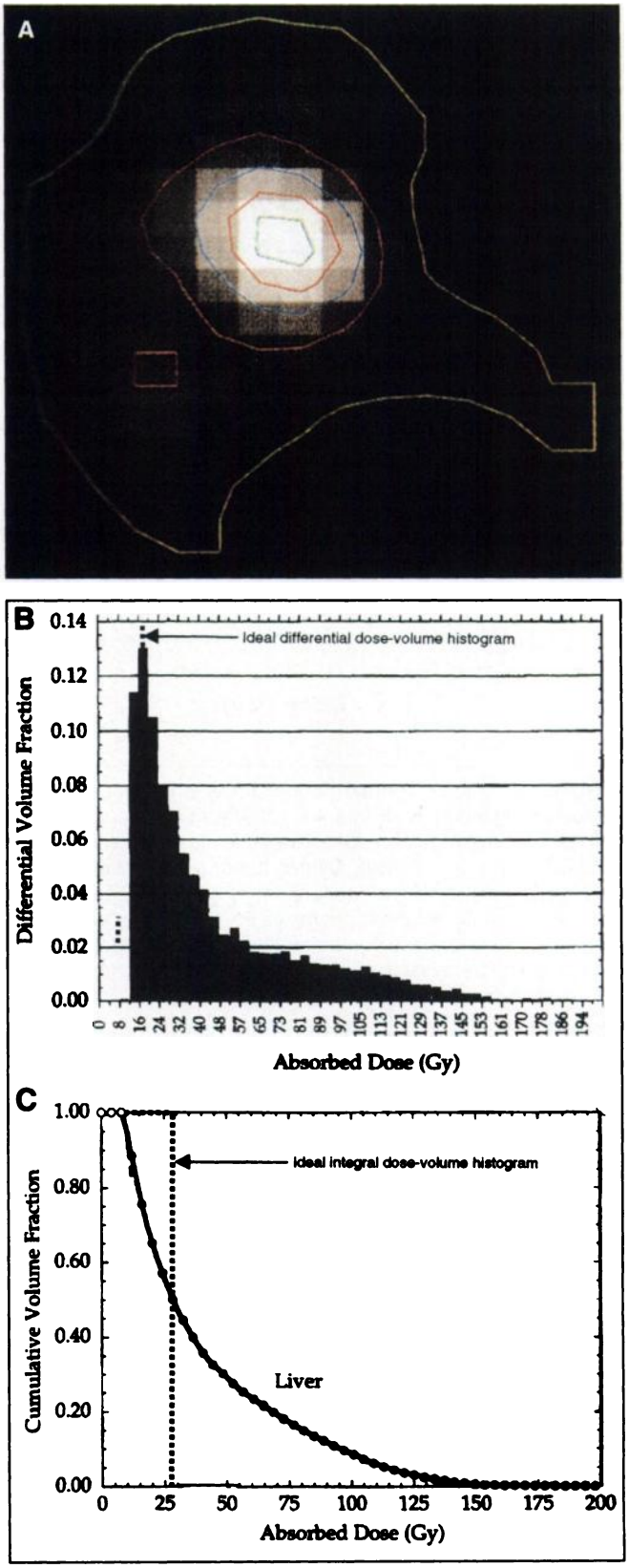

FIGURE 4. (A) Dose distribution, calculated by voxel S factor method and displayed as color-coded isodose contours superimposed on bremsstrahlung SPECT image of liver, after injection of ^{32}P chromic phosphate colloid (629 MBq [17 mCi]) into patient with nonresectable hepatic metastases. Isodose curves are shown for 10% (yellow), 30% (red), 50% (blue), 70% (orange), and 90% (green) of maximum voxel dose of 415 Gy (41,500 rad). (B) Corresponding differential dose-volume histogram. (C) Corresponding integral dose-volume histogram. Abscissa axes of histograms were truncated at 200 Gy (20,000 rad) because such small fraction of liver received doses in excess of this dose. As shown by dotted lines, "ideal" differential and integral dose-volume histogram would be vertical line and rectangle, respectively, indicating that entire tumor or tissue received uniform single dose. (Adapted with permission of (*29*).)

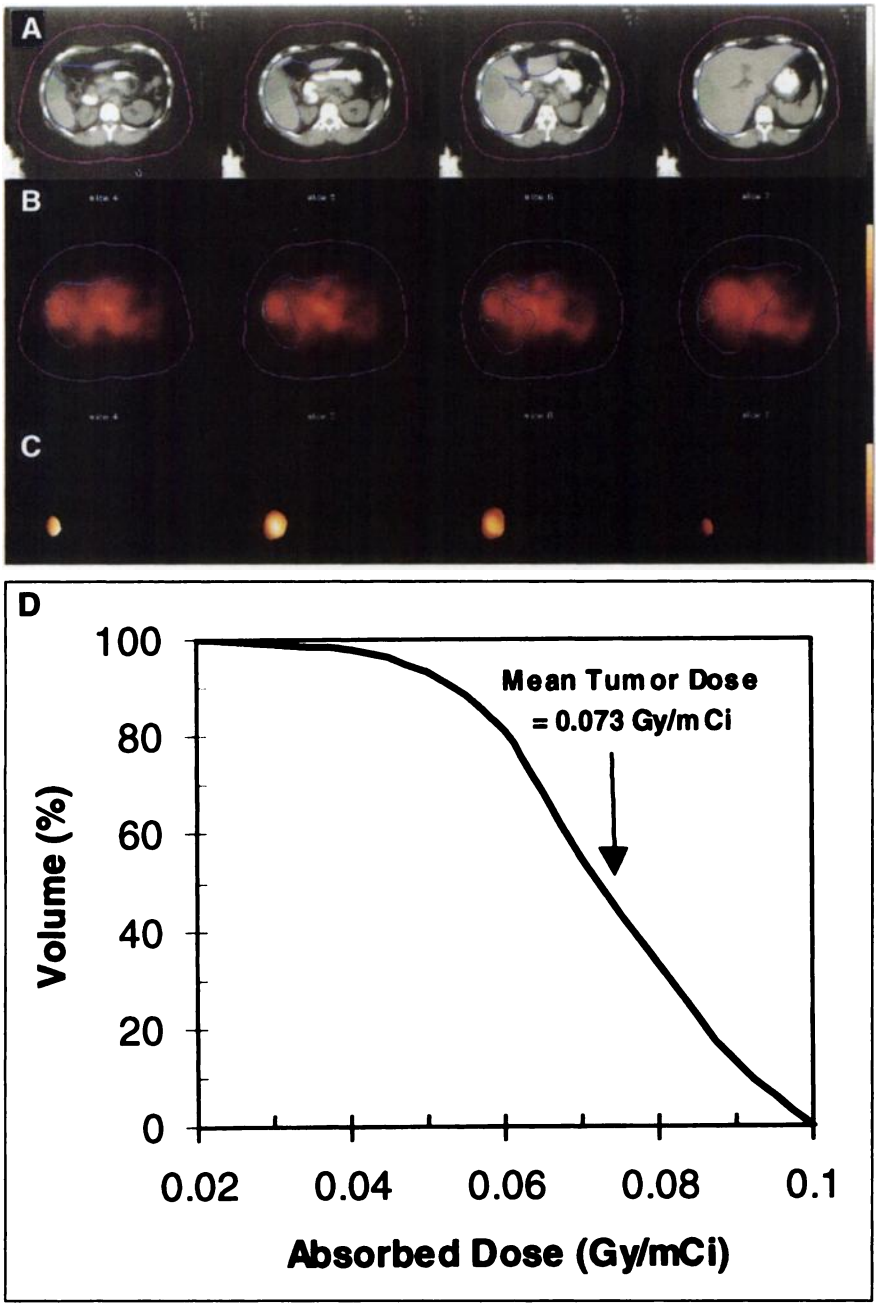

FIGURE 5. (A) Series of transverse CT images through liver (blue region of interest [ROI]) of patient with colorectal carcinoma and large hepatic metastasis (green ROI). (B) Corresponding series of transverse SPECT images after administration of ^{131}I-CC49 anti-TAG-72 murine monoclonal antibody (*132*) show liver activity delineated by blue ROI and tumor activity delineated by green ROI. (C) Dose distribution in hepatic metastasis, calculated by convolution of photon point-kernel with 3-dimensional activity distribution and by assuming complete intravoxel β-ray absorption. Images are displayed as "thermal" color coded, from black representing 0 dose to white representing maximum dose of 0.10 Gy–37 MBq (10 rad/mCi). (D) Integral dose–volume histogram. (Adapted with permission of (*114*).)

iodine therapy of hyperthyroidism or thyroid cancer in pregnant females. It is therefore critical to avoid radioiodine administration to the pregnant patient, even in diagnostic amounts.

Nursing Mothers

Diagnostic radiopharmaceuticals administered to lactating women can achieve high concentrations in breast milk and deliver potentially significant radiation doses to nursing infants (*125–128*). For example, the cumulative breast milk activity ranged from 0.03% to 27% ^{131}I administered to 6 women for thyroid uptake studies (*129*). Using a variety of dosimetric criteria (e.g., an effective dose equivalent to the nursing infant of 0.1 cSv [10.1 rem]), several authors have recommended different interruption periods before resuming breast-feeding after administration of radiopharmaceuticals. Although there is no absolute consensus, the following are representative of the published recommendations: 24 h after any administration of ^{99m}Tc, 2–4 wk after administration of ^{67}Ga-citrate, and permanently for the current nursing infant after any administration of ^{131}I (*125–128*).

Children

With the publication of the week by Christy and Eckerman (*21*), anthropomorphic models are now available for newborns and 1-, 5-, 10-, and 15-y-old children. Using the MIRDOSE 3.1 computer program and available kinetic data in conjunction with these models, Stabin and Gelfand (*130*)

estimated organ doses per unit administered activity for children of different ages for many commonly used diagnostic radiopharmaceuticals. Assuming typical values of administered activity, the doses, the effective dose equivalent, and the effective dose per procedure were tabulated. Comprehensive age-dependent dosimetric data are also presented in ICRP publication 53 (*20*).

REFERENCES

1. Stabin MG, Tagesson M, Thomas SR, Ljungberg M, Strand SE. Radiation dosimetry in nuclear medicine. *Appl Radiat Isot.* 1999;50:73–87.
2. Howell RW, Wessels BW, Loevinger R, et al. The MIRD perspective 1999. *J Nucl Med.* 1999;40:3S–10S.
3. Fisher DR. Radiation dosimetry for radioimmunotherapy: an overview of current capabilities and limitations. *Cancer.* 1994;73:905–911.
4. Goodhead D. Relationship of microdosimetric techniques to applications in biological systems. In: Kase K, Bjarngard B, Attix F, eds. *The Dosimetry of Ionizing Radiation.* Orlando, FL: Academic Press; 1987:1–89.
5. Rossi H. Microscopic energy distributions. In: Attix F, Roesch W, Tochlin E, eds. *Radiation Dosimetry.* New York, NY: Academic Press; 1968:43–92.
6. International Commission on Radiation Units and Measurements. *Microdosimetry.* ICRU report no. 36. Bethesda, MD: International Commission on Radiation Units and Measurements; 1983.
7. Fisher D. The microdosimetry of monoclonal antibodies labeled with alpha particles. In: Schlafke-Stelson A, Watson E, eds. *Proceedings of the Fourth International Radiopharmaceutical Dosimetry Symposium.* Oak Ridge, TN: United States Department of Energy and Oak Ridge Associated Universities; 1986:26–36.
8. Humm J. A microdosimetric model of astatine-211 labeled antibodies for radioimmunotherapy. *Int J Radiat Oncol Biol Phys.* 1987;13:1767–1773.
9. Humm JL, Roeske JC, Fisher DR, Chen GT. Microdosimetric concepts in radioimmunotherapy. *Med Phys.* 1993;20:535–541.
10. Kellerer A, Chmelevsky D. Criteria for the applicability of LET. *Radiat Res.* 1975;63:226–234.
11. National Council on Radiation Protection and Measurements. *SI Units in Radiation Protection and Measurements.* NCRP report no. 82. Bethesda, MD: National Council on Radiation Protection and Measurements; 1985.
12. International Commission on Radiological Protection. *Recommendations of the International Commission on Radiological Protection.* ICRP publication no. 60. Elmsford, NY: International Commission on Radiological Protection; 1977.
13. National Council on Radiation Protection and Measurements. *Limitations of Exposure to Ionizing Radiation.* NCRP report no. 91. Bethesda, MD: National Council on Radiation Protection and Measurements; 1987.
14. Zanzonico P. The fallacy of the chest x-ray as a basis for comparing radiogenic risks [abstract]. *J Nucl Med.* 1993;34(suppl):133P.
15. International Commission on Radiological Protection. *Recommendations of the International Commission on Radiological Protection.* ICRP publication no. 60. Elmsford, NY: International Commission on Radiological Protection; 1991.
16. National Council on Radiation Protection and Measurements. *Limitations of Exposure to Ionizing Radiation.* NCRP report no. 116. Bethesda, MD: National Council on Radiation Protection and Measurements; 1993.
17. Watson E. Foreword. *J Nucl Med.* 1999;40:1S–2S.
18. Loevinger R, Budinger T, Watson E, et al. *MIRD Primer for Absorbed Dose Calculations.* New York, NY: Society of Nuclear Medicine; 1991.
19. Loevinger R. The MIRD perspective. In: Adelstein S, Kassis A, Burt R, eds. *Dosimetry of Administered Radionuclides.* Washington, DC: American College of Nuclear Physicians/United States Department of Energy; 1989:29–43.
20. International Commission on Radiological Protection. *Radiation Dose to Patients from Radiopharmaceuticals.* ICRP publication no. 53. Oxford, UK: International Commission on Radiological Protection; 1983.
21. Cristy M, Eckerman K. *Specific Absorbed Fractions of Energy at Various Ages from Internal Photon Sources (I-VII).* Oak Ridge National Laboratory Report ORNL/TM-8381/V1–7. Springfield, VA: National Technical Information Service, United States Department of Commerce; 1987.
22. Snyder W, Ford M, Warner G. Estimates of absorbed fractions for monoenergetic photon sources uniformly distributed in various organs of a heterogeneous phantom: MIRD pamphlet no. 5. *J Nucl Med.* 1969;10(suppl 3):5–52.
23. Stabin MG. MIRDOSE: personal computer software for internal dose assessment in nuclear medicine. *J Nucl Med.* 1996;37:538–546.
24. Sgouros G, Bigler R, Zanzonico P. DOSCAL: a tumor-incorporating mean absorbed dose calculation program [abstract]. *J Nucl Med.* 1988;29(suppl):874.
25. Johnson T. MABDOS: a generalized program for internal dosimetry. *Comput Methods Programs Biomed.* 1988;37:159–167.
26. Johnson TK, McClure D, McCourt S. MABDOSE: part 1: Characterization of a general purpose dose estimation code. *Med Phys.* 1999;26:1389–1395.
27. Johnson TK, McClure D, McCourt S. MABDOSE: part 2: Validation of a general purpose dose estimation code. *Med Phys.* 1999;26:1396–1403.
28. Goddu S, Howell R, Bouchet L, et al. *MIRD Cellular S Factors: Self-Absorbed Dose per Unit Cumulated Activity for Selected Radionuclides and Monoenergetic Electrons and Alpha Particle Emitters Incorporated into Different Cell Compartments.* Reston, VA: Society of Nuclear Medicine; 1997:183.
29. Bolch WE, Bouchet LG, Robertson JS, et al. MIRD pamphlet No. 17: the dosimetry of nonuniform activity distributions—radionuclide S values at the voxel level. *J Nucl Med.* 1999;40:11S–36S.
30. Zanzonico P, Brill A, Becker D. Radiation dosimetry. In: Wagner H, Szabo Z, Buchanan J, eds. *Principles of Nuclear Medicine.* 2nd ed. Philadelphia, PA: WB Saunders Co.; 1995:106–134.
31. Werner S. Radioiodine. In: Werner S, Ingbar S, eds. *The Thyroid.* 4th ed. Hagerstown, MD: Harper & Row; 1978:827–835.
32. Marinelli L, Quimby E, Hine G. Dosage determination with radioactive isotopes: part 2. Practical considerations in therapy and protection. *AJR.* 1948;59:260–280.
33. Marinelli L, Quimby E, Hine G. Dosage determination with radioactive isotopes: part 1. Fundamental dosage formulae. *Nucleonics.* 1948;2:56–66.
34. Marinelli L, Quimby E, Hine G. Dosage determination with radioactive isotopes: part 2. Biological considerations and practical applications. *Nucleonics.* 1948;2:44–49.
35. Becker D, Hurley J. Radioiodine treatment of hyperthyroidism. In: Sandler M, Patton J, Coleman R, Gottschalk A, Wackers F, Hoffer P, eds. *Diagnostic Nuclear Medicine.* 3rd ed. Baltimore, MD: Williams & Wilkins; 1996:943–958.
36. Lazarus JH. Guidelines for the use of radioiodine in the management of hyperthyroidism: a summary. Prepared by the Radioiodine Audit Subcommittee of the Royal College of Physicians Committee on Diabetes and Endocrinology and the Research Unit of the Royal College of Physicians. *J R Coll Physicians Lond.* 1995;29:464–469.
37. Barandes M, Hurley J, Becker D. Implications of rapid intrathyroidal turnover for 131-I therapy: the small pool syndrome [abstract]. *J Nucl Med.* 1973;14(suppl):379.
38. DeNardo SJ, DeNardo GL, O'Grady LF, et al. Treatment of a patient with B-cell lymphoma by I-131 LYM-1 monoclonal antibodies. *Int J Biol Markers.* 1987;2:49–53.
39. DeNardo DA, DeNardo GL, Yuan A, et al. Prediction of radiation doses from therapy using tracer studies with iodine-131-labeled antibodies. *J Nucl Med.* 1996;37:1970–1975.
40. Sgouros G. Treatment planning for internal emitter therapy: methods, applications and clinical implications. In: Schlafke-Stelson A, Stabin M, Sparks R, eds. *Proceedings of the Sixth International Radiopharmaceutical Dosimetry Symposium.* ORISE 99–0164. Oak Ridge, TN: United States Department of Energy and Oak Ridge Associated Universities; 1999:13–25.
41. Zanzonico P, Edwards C, Sgouros G, et al. Practical dosimetry: quantitative imaging in radionuclide therapy. In: Adelstein S, Kassis A, Burt R, eds. *Dosimetry of Administered Radionuclides.* Washington, DC: American College of Nuclear Physicians/United States Department of Energy; 1989:275–294.
42. Erdi AK, Erdi YE, Yorke ED, Wessels BW. Treatment planning for radioimmunotherapy. *Phys Med Biol.* 1996;41:2009–2026.
43. Ott RJ. Imaging technologies for radionuclide dosimetry. *Phys Med Biol.* 1996;41:1885–1894.
44. Siegel JA, Thomas SR, Stubbs JB, et al. MIRD Pamphlet No. 16. Techniques for quantitative radiopharmaceutical biodistribution data acquisition and analysis for use in human radiation dose estimates. *J Nucl Med.* 1999;40:37S–61S.
45. Benua R, Cicale NR, Sonenberg M. The relation of radioiodine dosimetry to results and complications in the treatment of metastatic thyroid cancer. *AJR.* 1962;87:171–182.
46. Furhang EE, Larson SM, Buranapong P, Humm JL. Thyroid cancer dosimetry using clearance fitting. *J Nucl Med.* 1999;40:131–136.
47. Kaminski MS, Zasadny KR, Francis IR, et al. Radioimmunotherapy of B-cell lymphoma with [^{131}I]anti-B1 (anti-CD20) antibody. *N Engl J Med.* 1993;329:459–465.
48. Kaminski MS, Zasadny KR, Francis IR, et al. Iodine-131-anti-B1 radioimmunotherapy for B-cell lymphoma. *J Clin Oncol.* 1996;14:1974–1981.
49. Wahl RL, Zasadny KR, MacFarlane D, et al. Iodine-131 anti-B1 antibody for B-cell lymphoma: an update on the Michigan phase I experience. *J Nucl Med.* 1998;39(suppl):21S–27S.
50. Zasadny K, Gates V, Fisher S, Kaminski M, Wahl R. Correlation of dosimetric parameters with hematological toxicity after radioimmunotherapy of non-

Hodgkin's lymphoma with I-131 anti-B1: utility of a new parameter—Total body dose-lean [abstract]. *J Nucl Med.* 1995;36(suppl):214P.
51. Liu A, Williams LE, Demidecki AJ, Raubitschek AA, Wong JY. Modeling of tumor uptake to determine the time-dose-fractionation effect in radioimmunotherapy [letter]. *J Nucl Med.* 1994;35:1561–1564.
52. Odom-Maryon TL, Williams LE, Chai A, et al. Pharmacokinetic modeling and absorbed dose estimation for chimeric anti-CEA antibody in humans. *J Nucl Med.* 1997;38:1959–1966.
53. Sgouros G. Plasmapheresis in radioimmunotherapy of micrometastases: a mathematical modeling and dosimetrical analysis. *J Nucl Med.* 1992;33:2167–2179.
54. Sgouros G, Graham MC, Divgi CR, Larson SM, Scheinberg DA. Modeling and dosimetry of monoclonal antibody M195 (anti-CD33) in acute myelogenous leukemia. *J Nucl Med.* 1993;34:422–430.
55. Strand SE, Zanzonico P, Johnson TK. Pharmacokinetic modeling. *Med Phys.* 1993;20:515–527.
56. Willins JD, Sgouros G. Modeling analysis of platinum-195m for targeting individual blood-borne cells in adjuvant radioimmunotherapy. *J Nucl Med.* 1995;36:315–319.
57. Zanzonico P, Bigler R, Primus F, et al. A compartmental modeling approach to the radiation dosimetry of radiolabeled antibody. In: Schlafke-Stelson A, Watson E, eds. *Proceedings of the Fourth International Radiopharmaceutical Dosimetry Symposium.* Oak Ridge, TN: United States Department of Energy and Oak Ridge Associated Universities; 1986:421–445.
58. Furhang EE, Chui CS, Sgouros G. A Monte Carlo approach to patient-specific dosimetry. *Med Phys.* 1996;23:1523–1529.
59. Furhang EE, Chui CS, Kolbert KS, Larson SM, Sgouros G. Implementation of a Monte Carlo dosimetry method for patient-specific internal emitter therapy. *Med Phys.* 1997;24:1163–1172.
60. Erdi AK, Wessels BW, DeJager R, et al. Tumor activity confirmation and isodose curve display for patients receiving iodine-131-labeled 16.88 human monoclonal antibody. *Cancer.* 1994;73:932–944.
61. Erdi AK, Yorke ED, Loew MH, Erdi YE, Sarfaraz M, Wessels BW. Use of the fast Hartley transform for three-dimensional dose calculation in radionuclide therapy. *Med Phys.* 1998;25:2226–2233.
62. Giap HB, Macey DJ, Bayouth JE, Boyer AL. Validation of a dose-point kernel convolution technique for internal dosimetry. *Phys Med Biol.* 1995;40:365–381.
63. Giap HB, Macey DJ, Podoloff DA. Development of a SPECT-based three-dimensional treatment planning system for radioimmunotherapy. *J Nucl Med.* 1995;36:1885–1894.
64. Howell RW, Rao DV, Sastry KS. Macroscopic dosimetry for radioimmunotherapy: nonuniform activity distributions in solid tumors. *Med Phys.* 1989;16:66–74.
65. Humm JL. Dosimetric aspects of radiolabeled antibodies for tumor therapy. *J Nucl Med.* 1986;27:1490–1497.
66. Humm JL, Cobb LM. Nonuniformity of tumor dose in radioimmunotherapy. *J Nucl Med.* 1990;31:75–83.
67. Koral KF, Zasadny KR, Kessler ML, et al. CT-SPECT fusion plus conjugate views for determining dosimetry in iodine-131-monoclonal antibody therapy of lymphoma patients. *J Nucl Med.* 1994;35:1714–1720.
68. Kwok CS, Prestwich WV, Wilson BC. Calculation of radiation doses for nonuniformity distributed beta and gamma radionuclides in soft tissue. *Med Phys.* 1985;12:405–412.
69. Leichner PK, Kwok CS. Tumor dosimetry in radioimmunotherapy: methods of calculation for beta particles. *Med Phys.* 1993;20:529–534.
70. Liu A, Williams LE, Lopatin G, Yamauchi DM, Wong JY, Raubitschek AA. A radionuclide therapy treatment planning and dose estimation system. *J Nucl Med.* 1999;40:1151–1153.
71. Ljungberg M, Strand SE. Dose planning with SPECT. *Int J Cancer Suppl.* 1988;2:67–70.
72. Mayer R, Dillehay LE, Shao Y, et al. A new method for determining dose rate distribution from radioimmunotherapy using radiochromic media. *Int J Radiat Oncol Biol Phys.* 1994;28:505–513.
73. Sgouros G, Chiu S, Pentlow KS, et al. Three-dimensional dosimetry for radioimmunotherapy treatment planning. *J Nucl Med.* 1993;34:1595–1601.
74. Uchida I, Yamada Y, Oyamada H, Nomura E. Calculation algorithm of three-dimensional absorbed dose distribution due to in vivo administration of nuclides for radiotherapy [in Japanese]. *Kaku Igaku.* 1992;29:1299–1306.
75. Wessels BW, Yorke ED, Bradley EW. Dosimetry of heterogeneous uptake of radiolabeled antibody for radioimmunotherapy. *Front Radiat Ther Oncol.* 1990;24:104–108.
76. Akabani G, Hawkins W, Eckblade M, Leichner P. Patient-specific dosimetry using quantitative SPECT imaging and three-dimensional discrete Fourier transform convolution. *J Nucl Med.* 1997;38:308–314.
77. Liu A, Williams L, Wong J, Raubitschek A. A voxel source kernel (VSK) method for rapid, patient-specific dose estimates in radioimmunotherapy (RIT) [abstract]. *J Nucl Med.* 197;38(suppl):106P.
78. Adelstein S, Kassis A, Sastry K. Cellular vs. organ approaches to dose estimates. In: Schlafke-Stelson A, Watson E, eds. *Proceedings of the Fourth International Radiopharmaceutical Dosimetry Symposium.* Oak Ridge, TN: United States Department of Energy and Oak Ridge Associated Universities; 1986:13–25.
79. Goddu SM, Rao DV, Howell RW. Multicellular dosimetry for micrometastases: dependence of self-dose versus cross-dose to cell nuclei on type and energy of radiation and subcellular distribution of radionuclides. *J Nucl Med.* 1994;35:521–530.
80. Griffiths GL, Govindan SV, Sgouros G, Ong GL, Goldenberg DM, Mattes MJ. Cytotoxicity with Auger electron-emitting radionuclides delivered by antibodies. *Int J Cancer.* 1999;81:985–992.
81. Humm JL, Howell RW, Rao DV. Dosimetry of Auger-electron-emitting radionuclides: report no. 3 of AAPM Nuclear Medicine Task Group No. 6. *Med Phys.* 1994;21:1901–1915. [Published correction appears in *Med Phys.* 1995;22:1837.]
82. Humm JL, Macklis RM, Lu XQ, et al. The spatial accuracy of cellular dose estimates obtained from 3D reconstructed serial tissue autoradiographs. *Phys Med Biol.* 1995;40:163–180.
83. Macklis RM, Lin JY, Beresford B, Atcher RW, Hines JJ, Humm JL. Cellular kinetics, dosimetry, and radiobiology of alpha-particle radioimmunotherapy: induction of apoptosis. *Radiat Res.* 1992;130:220–226.
84. O'Donoghue JA, Wheldon TE. Targeted radiotherapy using Auger electron emitters. *Phys Med Biol.* 1996;41:1973–1992.
85. O'Donoghue JA. Strategies for selective targeting of Auger electron emitters to tumor cells. *J Nucl Med.* 1996;37(suppl):3S–6S.
86. Wrenn ME, Howells GP, Hairr LM, Paschoa AS. Auger electron dosimetry. *Health Phys.* 1973;24:645–653.
87. Yorke ED, Williams LE, Demidecki AJ, Heidorn DB, Roberson PL, Wessels BW. Multicellular dosimetry for beta-emitting radionuclides: autoradiography, thermoluminescent dosimetry and three-dimensional dose calculations. *Med Phys.* 1993;20:543–550.
88. Zalutsky MR, Stabin MG, Larsen RH, Bigner DD. Tissue distribution and radiation dosimetry of astatine-211-labeled chimeric 81C6, an alpha-particle-emitting immunoconjugate. *Nucl Med Biol.* 1997;24:255–261.
89. Kassis AI, Adelstein SJ, Haydock C, Sastry KS. Radiotoxicity of ^{75}Se and ^{35}S: theory and application to a cellular model. *Radiat Res.* 1980;84:407–425.
90. Kassis AI, Adelstein SJ, Haydock C, Sastry KS, McElvany KD, Welch MJ. Lethality of Auger electrons from the decay of bromine-77 in the DNA of mammalian cells. *Radiat Res.* 1982;90:362–373.
91. Kassis AI, Adelstein SJ, Haydock C, Sastry KS. Thallium-201: an experimental and a theoretical radiobiological approach to dosimetry. *J Nucl Med.* 1983;24:1164–1175.
92. Kassis AI, Sastry KS, Adelstein SJ. Intracellular distribution and radiotoxicity of chromium-51 in mammalian cells: Auger-electron dosimetry. *J Nucl Med.* 1985;26:59–67.
93. Kassis AI, Fayad F, Kinsey BM, Sastry KS, Taube RA, Adelstein SJ. Radiotoxicity of ^{125}I in mammalian cells. *Radiat Res.* 1987;111:305–318.
94. Kassis AI, Sastry KS, Adelstein SJ. Kinetics of uptake, retention, and radiotoxicity of ^{125}IUdR in mammalian cells: implications of localized energy deposition by Auger processes. *Radiat Res.* 1987;109:78–89.
95. Kassis AI. The MIRD approach: remembering the limitations. *J Nucl Med.* 1992;33:781–782.
96. Makrigiorgos GM, Adelstein SJ, Kassis AI. Limitations of conventional internal dosimetry at the cellular level. *J Nucl Med.* 1989;30:1856–1864.
97. Siegel J, Wessels B, Watson E, et al. Bone marrow dosimetry and toxicity in radioimmunotherapy. *Antibody Immunocon Radiopharm.* 1990;3:213–223.
98. DeNardo GL, DeNardo SJ, Macey DJ, Shen S, Kroger LA. Overview of radiation myelotoxicity secondary to radioimmunotherapy using ^{131}I-Lym-1 as a model. *Cancer.* 1994;73:1038–1048.
99. Bigler R, Zanzonico P, Primus F, et al. Bone marrow dosimetry for monoclonal antibody therapy. In: Schlafke-Stelson A, Watson E, eds. *Proceedings of the Fourth International Radiopharmaceutical Dosimetry Symposium.* Oak Ridge, TN: United States Department of Energy and Oak Ridge Associated Universities; 1986:535–544.
100. Sgouros G. Bone marrow dosimetry for radioimmunotherapy: theoretical considerations. *J Nucl Med.* 1993;34:689–694.
101. Macey DJ, DeNardo SJ, DeNardo GL, DeNardo DA, Shen S. Estimation of radiation absorbed doses to the red marrow in radioimmunotherapy. *Clin Nucl Med.* 1995;20:117–125.
102. DeNardo DA, DeNardo GL, O'Donnell RT, et al. Imaging for improved prediction of myelotoxicity after radioimmunotherapy. *Cancer.* 1997;80:2558–2566.

103. Lim S, DeNardo GL, DeNardo DA, O'Donnell RT, Yuan A, DeNardo SJ. Prediction of myelotoxicity using semi-quantitative marrow image scores. *J Nucl Med.* 1997;38:1749–1753.
104. Lim SM, DeNardo GL, DeNardo DA, et al. Prediction of myelotoxicity using radiation doses to marrow from body, blood and marrow sources. *J Nucl Med.* 1997;38:1374–1378.
105. Zanzonico P, Sgouros G. Predicting myelotoxicity in radioimmunotherapy: what does dosimetry contribute? *J Nucl Med.* 1997;38:1753–1754.
106. Sgouros G, Divgi C, Scott A, Williams J, Larson S. Hematologic toxicity in radioimmunotherapy: an evaluation of different predictive measures [abstract]. *J Nucl Med.* 1996;37(suppl):43P–44P.
107. Sgouros G, Deland D, Loh A, Divgi C, Larson S. Marrow and whole-body absorbed dose vs. marrow toxicity following ^{131}I-G250 antibody therapy in patients with renal cell carcionoma [abstract]. *J Nucl Med.* 1997;38(suppl):252P.
108. O'Donoghue JA. Implications of nonuniform tumor doses for radioimmunotherapy. *J Nucl Med.* 1999;40:1337–1341.
109. Humm JL, Macklis RM, Bump K, Cobb LM, Chin LM. Internal dosimetry using data derived from autoradiographs. *J Nucl Med.* 1993;34:1811–1817.
110. Sgouros G, Barest G, Thekkumthala J, et al. Treatment planning for internal radionuclide therapy: three-dimensional dosimetry for nonuniformly distributed radionuclides. *J Nucl Med.* 1990;31:1884–1891.
111. Tagesson M, Ljungberg M, Strand SE. A Monte-Carlo program converting activity distributions to absorbed dose distributions in a radionuclide treatment planning system. *Acta Oncol.* 1996;35:367–372.
112. Scott AM, Macapinlac H, Zhang JJ, et al. Clinical applications of fusion imaging in oncology. *Nucl Med Biol.* 1994;21:775–784.
113. Scott AM, Macapinlac H, Zhang J, et al. Image registration of SPECT and CT images using an external fiduciary band and three-dimensional surface fitting in metastatic thyroid cancer. *J Nucl Med.* 1995;36:100–103.
114. Kolbert KS, Sgouros G, Scott AM, et al. Implementation and evaluation of patient-specific three-dimensional internal dosimetry. *J Nucl Med.* 1997;38:301–308.
115. Koral KF, Lin S, Fessler JA, Kaminski MS, Wahl RL. Preliminary results from intensity-based CT-SPECT fusion in I-131 anti-B1 monoclonal-antibody therapy of lymphoma. *Cancer.* 1997;80:2538–2544.
116. Smith EM, Warner GG. Estimates of radiation dose to the embryo from nuclear medicine procedures. *J Nucl Med.* 1976;17:836–839.
117. Watson E, Stabin M, Eckerman K, Cristy M, Ryman J, Davis J. Model 2: mathematical models of the pregnant woman at the end of the first and third trimesters. In: Schlafke-Stelson A, Watson E, eds. *Proceedings of the Fourth International Radiopharmaceutical Dosimetry Symposium.* Oak Ridge, TN: United States Department of Energy and Oak Ridge Associated Universities; 1986:89–104.
118. Hedrick WR, DiSimone RN, Wolf BH, Langer A. Absorbed dose to the fetus during bone scintigraphy. *Radiology.* 1988;168:245–248.
119. Cloutier RJ, Smith SA, Watson EE, Snyder WS, Warner GG. Dose to the fetus from radionuclides in the bladder. *Health Phys.* 1973;25:147–161.
120. Husak V, Wiedermann M. Radiation absorbed dose estimates to the embryo from some nuclear medicine procedures. *Eur J Nucl Med.* 1980;5:205–207.
121. Marcus CS, Mason GR, Kuperus JH, Mena I. Pulmonary imaging in pregnancy: maternal risk and fetal dosimetry. *Clin Nucl Med.* 1985;10:1–4.
122. Ponto JA. Fetal dosimetry from pulmonary imaging in pregnancy: revised estimates. *Clin Nucl Med.* 1986;11:108–109.
123. Stabin MG, Watson EE, Marcus CS, Salk RD. Radiation dosimetry for the adult female and fetus from iodine-131 administration in hyperthyroidism. *J Nucl Med.* 1991;32:808–813.
124. Zanzonico P, Becker D. Radiation hazards in children born to mothers exposed to ^{131}I. In: Beckers C, Reinwein D, eds. *The Thyroid and Pregnancy.* Stuttgart, Germany: Schattauer; 1991:189–202.
125. Ahlgren L, Ivarsson S, Johansson L, Mattsson S, Nosslin B. Excretion of radionuclides in human breast milk after the administration of radiopharmaceuticals. *J Nucl Med.* 1985;26:1085–1090.
126. Mountford PJ, Coakley AJ. A review of the secretion of radioactivity in human breast milk: data, quantitative analysis and recommendations. *Nucl Med Commun.* 1989;10:15–27.
127. Romney B, Nickoloff E, Esser P, Alderson P. Radionuclide administration to nursing mothers: mathematically derived guidelines. *Radiology.* 1986;160:549–554.
128. Rubow S, Klopper J, Wasserman H, Baard B, van Niekerk M. The excretion of radiopharmaceuticals in human breast milk: additional data and dosimetry. *Eur J Nucl Med.* 1994;21:144–153.
129. Weaver J, Kamm M, Dobson R. Excretion of radioiodine in human milk. *JAMA.* 1960:872–875.
130. Stabin MG, Gelfand MJ. Dosimetry of pediatric nuclear medicine procedures. *Q J Nucl Med.* 1998;42:93–112.
131. Sgouros G, Jureidini IM, Scott AM, Graham MC, Larson SM, Scheinberg DA. Bone marrow dosimetry: regional variability of marrow-localizing antibody. *J Nucl Med.* 1996;37:695–698.
132. Divgi CR, Scott AM, Dantis L, et al. Phase I radioimmunotherapy trial with iodine-131-CC49 in metastatic colon carcinoma. *J Nucl Med.* 1995;36:586–592.